Title

Quinolone-mediated metabolic cross-feeding develops aluminium tolerance in soil microbial consortia.

Journal

Nature Communications, 15(1)

Authors

Ma, Zhiyuan
Jiang, Meitong
Liu, Chaoyang
et al.

Publication Date

2024-11-22

DOI

10.1038/s41467-024-54616-0

Peer reviewed

nature communications

Article

https://doi.org/10.1038/s41467-024-54616-0

Quinolone-mediated metabolic cross-feeding develops aluminium tolerance in soil microbial consortia

Received: 20 May 2024

Accepted: 15 November 2024

Published online: 22 November 2024

Check for updates

Zhiyuan Ma[1,10], Meitong Jiang[1,2,10], Chaoyang Liu[1], Ertao Wang[3], Yang Bai[4], Mengting Maggie Yuan[5], Shengjing Shi[6], Jizhong Zhou[7], Jixian Ding[1], Yimei Xie[1,2], Hui Zhang[1], Yan Yang[1,8], Renfang Shen[1], Thomas W. Crowther[9], Jiabao Zhang[1] & Yuting Liang[1,2]

Aluminium (Al)-tolerant beneficial bacteria confer resistance to Al toxicity to crops in widely distributed acidic soils. However, the mechanism by which microbial consortia maintain Al tolerance under acid and Al toxicity stress remains unknown. Here, we demonstrate that a soil bacterial consortium composed of *Rhodococcus erythropolis* and *Pseudomonas aeruginosa* exhibit greater Al tolerance than either bacterium alone. *P. aeruginosa* releases the quorum sensing molecule 2-heptyl-1H-quinolin-4-one (HHQ), which is efficiently degraded by *R. erythropolis*. This degradation reduces population density limitations and further enhances the metabolic activity of *P. aeruginosa* under Al stress. Moreover, *R. erythropolis* converts HHQ into tryptophan, promoting the synthesis of peptidoglycan, a key component for cell wall stability, thereby improving the Al tolerance of *R. erythropolis*. This study reveals a metabolic cross-feeding mechanism that maintains microbial Al tolerance, offering insights for designing synthetic microbial consortia to sustain food security and sustainable agriculture in acidic soil regions.

Interspecies interactions serve as the primary impetus for microbial community activity, significantly influencing community composition, structure, and function[1]. In natural habitats, microbial communities often acquire essential nutrients and maintain biodiversity through metabolic cross-feeding mechanisms[2,3]. Microbial producers synthesize an array of extracellular molecules, encompassing exoenzymes and vital metabolites such as sugars, organic acids, and amino acids, which can subsequently be utilized by neighboring microbes[2–4]. Microorganisms augment performance at the community level in various contexts through emergent properties that arise from complex interactions[5]. This effect surpasses the aggregate of their individual contributions[6]. Central to these microbial interactions is quorum sensing (QS), a mechanism that can modulate nutrient uptake and metabolic processes, thereby shaping microbial responses to dynamic environments[7,8]. In the soil environment, where multiple stringent constraints exist, microorganisms appear capable of preserving functionality and biodiversity from the individual to the community level through cooperative strategies. Non-competitive metabolite pools are thus advantageous for fostering constructive metabolic interactions[9,10]. For instance, *Bacillus* and *Delftia* maintain

[1]State Key Laboratory of Soil and Sustainable Agriculture, Institute of Soil Science, Chinese Academy of Sciences, Nanjing, China. [2]University of Chinese Academy of Sciences, Beijing, China. [3]National Key Laboratory of Plant Molecular Genetics, CAS Center for Excellence in Molecular Plant Sciences, Institute of Plant Physiology and Ecology, SIBS, Chinese Academy of Sciences, Shanghai, China. [4]School of Life Sciences, Peking University, Beijing, China. [5]Department of Environmental Science, Policy and Management, University of California, Berkeley, CA, USA. [6]AgResearch Ltd, Lincoln Science Centre, Lincoln, New Zealand. [7]Department of Microbiology and Plant Biology, University of Oklahoma, Norman, OK, USA. [8]School of Environmental Science and Engineering, Changzhou University, Changzhou, China. [9]Department of Environmental Systems Science, Institute of Integrative Biology, ETH, Zurich, Switzerland. [10]These authors contributed equally: Zhiyuan Ma, Meitong Jiang. e-mail: ytliang@issas.ac.cn

their survival and competitive edge in soil through a mutualistic relationship facilitated by pyruvate exchange, which also plays a role in modulating the soil arsenic cycle[11].

Aluminium (Al) toxicity represents a significant stress factor in acidic soils and is considered the second most common abiotic stress after drought for crops worldwide[12]. When the pH falls below 5.5, substantial amounts of Al^{3+} are liberated into the soil solution[13]. This can result in microbial cell wall relaxation, membrane rupture, and leakage of cellular compounds, consequently impeding microbial activity and, in severe cases, leading to cell death[14]. Al-tolerant microorganisms have adapted to combat Al toxicity through various mechanisms, such as fortifying their cell walls and excreting organic acid to chelate Al^{3+}[15,16]. In addition to individual tolerance capabilities and survival mechanisms, diverse interactions among microorganisms enable them to maintain community activity, diversity, and stability when faced with environmental stress[17]. This may help elucidate previous observations that acidic soils support a wide distribution of microorganisms exhibiting varying sensitivities to Al[18]. Synthetic microbial consortia, derived from natural microbial communities, have been shown to outperform individual microbes in our previous study[18]. However, a significant knowledge gap remains regarding the mechanisms through which these microorganisms coexist and withstand Al toxicity stress.

In a previous study, we established a synthetic microbial community (SynCom) in acidic soils comprising two bacterial strains—*Rhodococcus erythropolis* and *Pseudomonas aeruginosa*—with different levels of tolerance to Al[18]. SynCom has demonstrated robust co-colonization in field settings and has outperformed individual strains in promoting plant growth[18]. Consequently, we hypothesize that SynCom members can bolster community-level Al tolerance and augment plant growth promotion via cross-feeding mechanisms.

Here, we show that the SynCom exhibits greater Al tolerance than either *R. erythropolis* or *P. aeruginosa* alone. *P. aeruginosa* produces the secondary metabolite 2-heptyl-1H-quinolin-4-one (HHQ), which is efficiently degraded by *R. erythropolis*. This degradation reduces QS limitations, enhancing *P. aeruginosa*'s metabolic activity under Al stress. Furthermore, *R. erythropolis* converts HHQ into tryptophan via the chorismate biosynthesis pathway, which promotes peptidoglycan synthesis, improving cell wall stability and Al tolerance in *R. erythropolis*. Our study elucidates the mechanisms of interspecies Al tolerance, which is fundamental for enhancing microbial community functions and offers valuable theoretical insights for the design and development of SynCom for sustainable agricultural applications.

Results

SynCom enhances individual species effects

A SynCom consisting of two Al-tolerant strains, *R. erythropolis* (Rh) and *P. aeruginosa* (Ps), denoted as RP, significantly enhanced both the biomass and yield of rice compared to single-species inoculation (Rh and Ps) or no inoculation (CK) under acidic Al toxicity conditions in the field (Supplementary Fig. 1a, b). At the mature grain stage, the shoot fresh weight under the RP treatment increased by 21.32% and 34.98% compared to that under the Rh and Ps treatments, respectively, and the grain yield significantly increased by 21.00% and 26.27%, respectively (Supplementary Fig. 1c). A pot experiment further proved that compared with single inoculation, the RP treatment led to greater increases in rice growth during the elongation stage, as well as in biomass and yield at maturity (Supplementary Fig. 2). These results are consistent with previous findings[18]. Besides, the Al content in the roots was the lowest with SynCom inoculation, followed by Ps, Rh, and CK treatments (Supplementary Fig. 3). Building on these validations, we further aimed to unravel the underlying cooperative mechanisms that contribute to the superior performance of co-culture over mono-culture in promoting plant growth.

In the pot experiment, SynCom members demonstrated higher colonization abundance and stable colonization efficiency compared to single inoculations, as determined by quantitative real-time polymerase chain reaction (qRT–PCR). Specifically, SynCom significantly enhanced the bacterial abundance, with a 1.50-fold increase in response to Rh (RP versus Rh) and a 1.42-fold increase in total microbial abundance in response to Ps (RP versus Ps) (Fig. 1a). Moreover, the co-cultured products markedly increased the absolute abundance of *R. erythropolis* by 1.29-fold (RP versus Rh) and *P. aeruginosa* by 2.30-fold (RP versus Ps) (Fig. 1b). Using fluorescent in situ hybridization (FISH), we observed that while mono-inoculation of *P. aeruginosa* inhibited the biomass of native *R. erythropolis* by 2.91-fold compared with CK treatment, co-inoculation enhanced the biomass of *R. erythropolis* by 1.71-fold (Fig. 1c and Supplementary Fig. 4).

Interestingly, we confirmed that the metabolic dynamics of *R. erythropolis* and *P. aeruginosa* under acidic Al stress was enhanced in co-culture condition compared to mono-cultures. In single-cell Raman spectroscopy combined with reverse heavy water labeling (Reverse-Raman-D_2O) (Fig. 1d), the substitution of labeled deuterium was proportional to cellular metabolic activity. Cells with a lower $C–D_{ratio}$ indicate heightened metabolic activity under Al stress, while cells with a significantly higher $C–D_{ratio}$ suggest reduced activity under Al stress. Our investigations revealed that the two bacterial species exhibited differential resistance to Al stress when cultured in the minimal medium at pH 4.0 (Supplementary Fig. 5). Regardless of cultured individually or together, the metabolic activity of *P. aeruginosa* remained unchanged across varying concentrations of Al^{3+} (Fig. 1e). The metabolic activity of *P. aeruginosa* was significantly augmented in the presence of *R. erythropolis*. In contrast, as the concentrations of Al^{3+} increased from 0 mM to 1.0 mM, we observed a 13.49%–28.46% decrease in the metabolic activity of *R. erythropolis* in the mono-culture. The metabolic activity of *R. erythropolis* increased by 18.76%–25.42% when co-cultured. Furthermore, we confirmed that co-culture substantially improved the phosphorus (P)-solubilizing efficiency under acidic Al stress compared to mono-cultures (Supplementary Fig. 6, Supplementary Note 1). Together with our previous findings[18], co-culture has enhanced the Al resistance of SynCom members, and this increased activity has further augmented the P-solubilizing ability of SynCom.

We subsequently determined the growth curves of the two bacterial species during co-culture under 0.1 mM Al^{3+} conditions (pH 4.0) (Fig. 1f). *P. aeruginosa* in mono-culture reached a density-dependent limit soon after 12 h, with a decrease in population from 5.72×10^9 copies mL^{-1} to 1.67×10^9 copies mL^{-1}. When co-cultured with *R. erythropolis*, the cell density of *P. aeruginosa* at 12 h was 1.53 times greater than that in the mono-culture, reaching a stationary phase at 6.77×10^9 copies mL^{-1}. In addition, *R. erythropolis* in the co-culture was significantly greater (7.94 times greater) than that in the mono-culture (7.65×10^9 copies mL^{-1}) at 18 h.

These findings indicated a mutualistic benefit between the two bacterial strains during their coexistence. Specifically, the Al tolerance of *R. erythropolis* was significantly enhanced when co-cultured with *P. aeruginosa*, while *P. aeruginosa* experienced a mitigated density-dependent growth limitation. Consequently, we inferred that the two species may engage in synergistic metabolic interactions, possibly involving the sharing or exchange of metabolic products, which facilitated their adaptation to Al stress.

Interspecies interactions mediated by quinolones

To elucidate the metabolic substrates involved in cross-feeding between *R. erythropolis* and *P. aeruginosa*, we identified their metabolites under both mono-culture and co-culture conditions cultivated in minimal media under Al stress (pH 4.0). We analysed 19 metabolic substances, including sugars, long-chain fatty acids, and aromatic compounds, using single quadrupole gas chromatography–mass spectrometry (GC–MS) (Supplementary Data 1). 2-heptyl-1H-quinolin-4-one (HHQ), a key QS signaling molecule, was uniquely detected in

https://doi.org/10.1038/s41467-024-54616-0

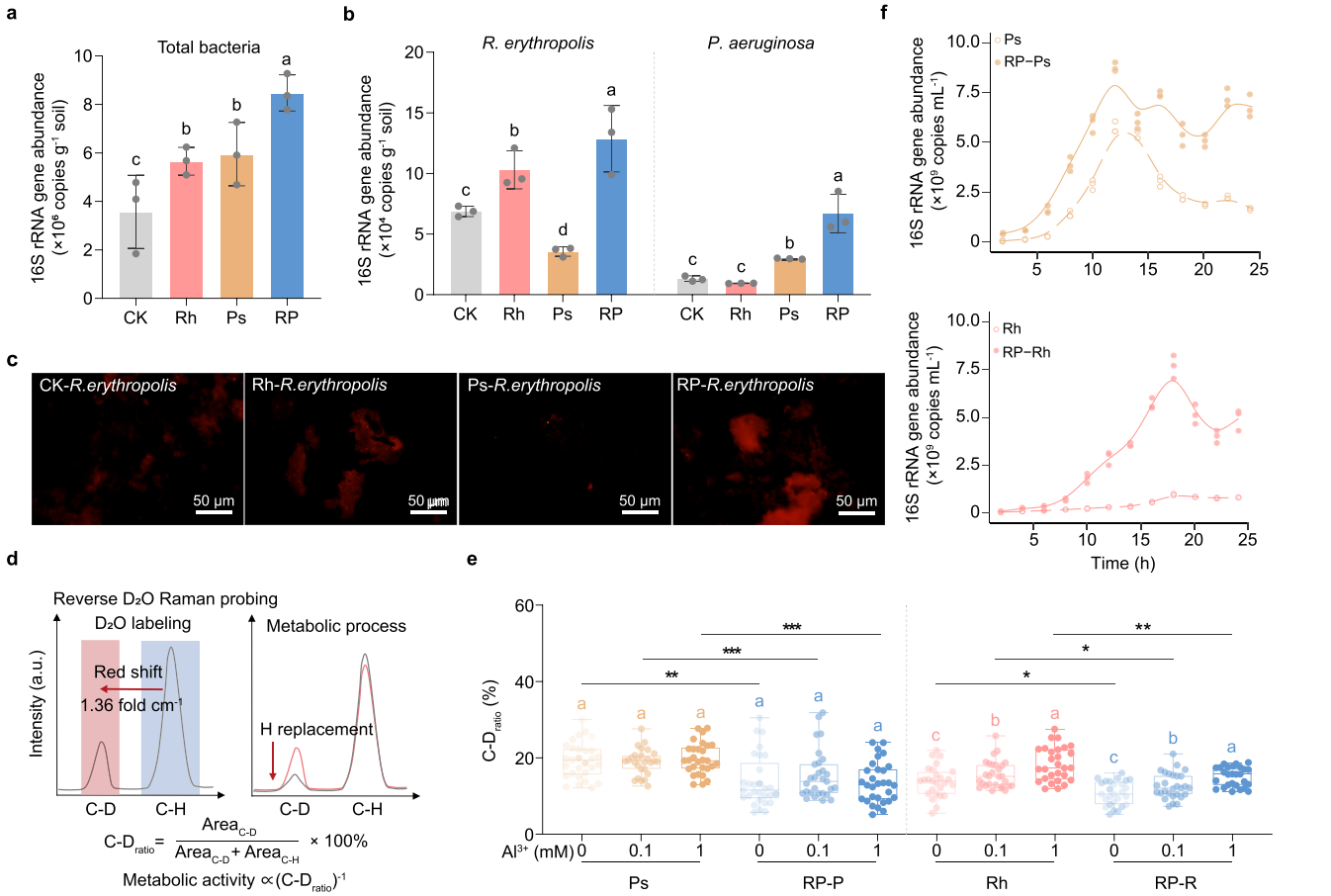

Fig. 1 | Changes in the community density and activity of *R. erythropolis* and *P. aeruginosa* under mono-culture and co-culture conditions. The absolute abundance of total bacteria (**a**), *R. erythropolis*, and *P. aeruginosa* (**b**) in the rice rhizosphere soil ($n = 3$ rhizosphere soil samples). **c** Fluorescence in situ hybridization of *R. erythropolis* in rhizosphere soil. The scale bar is 50 μm. The fluorescence experiment was independently repeated three times. **d** Single-cell reverse heavy water labeling principle and calculation formula for metabolic activity ($C–D_{ratio}$). $Area_{C–D}$ represents the integral area of the Raman peak at 2040–2300 cm^{-1} after the redshift of heavy water substitution (C–D), and $Area_{C–H}$ represents the integral area of the unsubstituted C–H at 2800–3100 cm^{-1}. **e** Metabolic activity of *R. erythropolis* and *P. aeruginosa* under mono-culture and co-culture conditions with different Al^{3+} concentrations (pH 4.0) ($n = 30$ individual cells). **f** Absolute abundance of *P. aeruginosa* and *R. erythropolis* over time under mono-culture and co-culture treatments ($n = 3$ biological replicates). In (**a**, **b**), the bars represent the means ± s.d. In (**e**) the horizontal bars within the box plots represent medians, the tops and bottoms of the boxes represent the 75th and 25th percentiles, respectively, and the upper and lower whiskers extend to the maximum and minimum values, respectively. In (**a**, **b**, **e**), different letters indicate significant differences ($P < 0.05$, One-way ANOVA, two-sided Fisher's LSD test). In (**e**), the significance labels are color-coded to match their corresponding treatments. The two-sided unpaired *t*-test was used for statistical significance testing. $^{*}P < 0.05$, $^{**}P < 0.01$, and $^{***}P < 0.001$. CK non-inoculation, Rh inoculation with *R. erythropolis*, Ps inoculation with *P. aeruginosa*, RP inoculation with *R. erythropolis* and *P. aeruginosa*, RP-R *R. erythropolis* in co-culture, RP-P *P. aeruginosa* in co-culture. Source data are provided as a Source Data file.

mono-cultured *P. aeruginosa* but was absent in mono-cultured *R. erythropolis* (Fig. 2a). Moreover, compared to the mono-culture of *P. aeruginosa*, the concentration of HHQ in the co-culture was reduced by approximately half (Fig. 2a).

We then employed semiflexible molecular docking simulations to calculate the binding free energy of each metabolite with the Quorum-sensing degradation regulator[19] (QsdR) and multiple virulence factor regulator (mvfR)[20] transcription factor proteins (Methods). Among all the detected substances, HHQ exhibited the lowest binding free energy with both QsdR and mvfR (−7.39 kcal mol^{-1} and −6.15 kcal mol^{-1}, respectively), suggesting a greater likelihood of binding to the target proteins (Fig. 2b). This preferential binding may be attributed to the unique quinolone framework structure of HHQ, which features an electron-withdrawing phenol group and an electron-donating pyridine group, facilitating easier binding to protein sites (Fig. 2c).

Subsequently, we quantified and confirmed the production of HHQ by *P. aeruginosa* and its degradation by *R. erythropolis* in pure cultures. After 12 h of incubation under 0.1 mM added Al^{3+} concentration in minimal media, HHQ was undetectable in *R. erythropolis* mono-culture but remained at a concentration of 1.0 ± 0.05 μg mL^{-1} in *P. aeruginosa* mono-culture. In co-cultures, the concentration of HHQ significantly decreased to 0.42 ± 0.14 μg mL^{-1} (Fig. 2d). Moreover, the mono-cultured *R. erythropolis* exhibited strong metabolic activity towards HHQ during the 8-h incubation period with increasing Al^{3+} concentrations (Fig. 2e). Correspondingly, the production and degradation of HHQ were examined in rice-cultivated acidic soil under both natural and sterilized conditions, as well as in a sterilized clay-based system. These experiments proved the efficient ability of *R. erythropolis* to degrade HHQ, both in liquid medium and soil matrix (Supplementary Figs. 7 and 8, Supplementary Note 2).

Together, our findings revealed a crucial metabolic link between the two bacterial species in the co-culture system. The HHQ produced by *P. aeruginosa* not only participates in the regulation of QS processes in microbial populations but also may be exploited by *R. erythropolis* as a nutritional resource, enhancing its capacity to withstand Al toxicity stress.

R. erythropolis degrades HHQ to augment cell wall biosynthesis

Based on a transcriptomic analysis, we identified the top 10 enriched metabolic pathways for differentially expressed genes (DEGs) between

https://doi.org/10.1038/s41467-024-54616-0

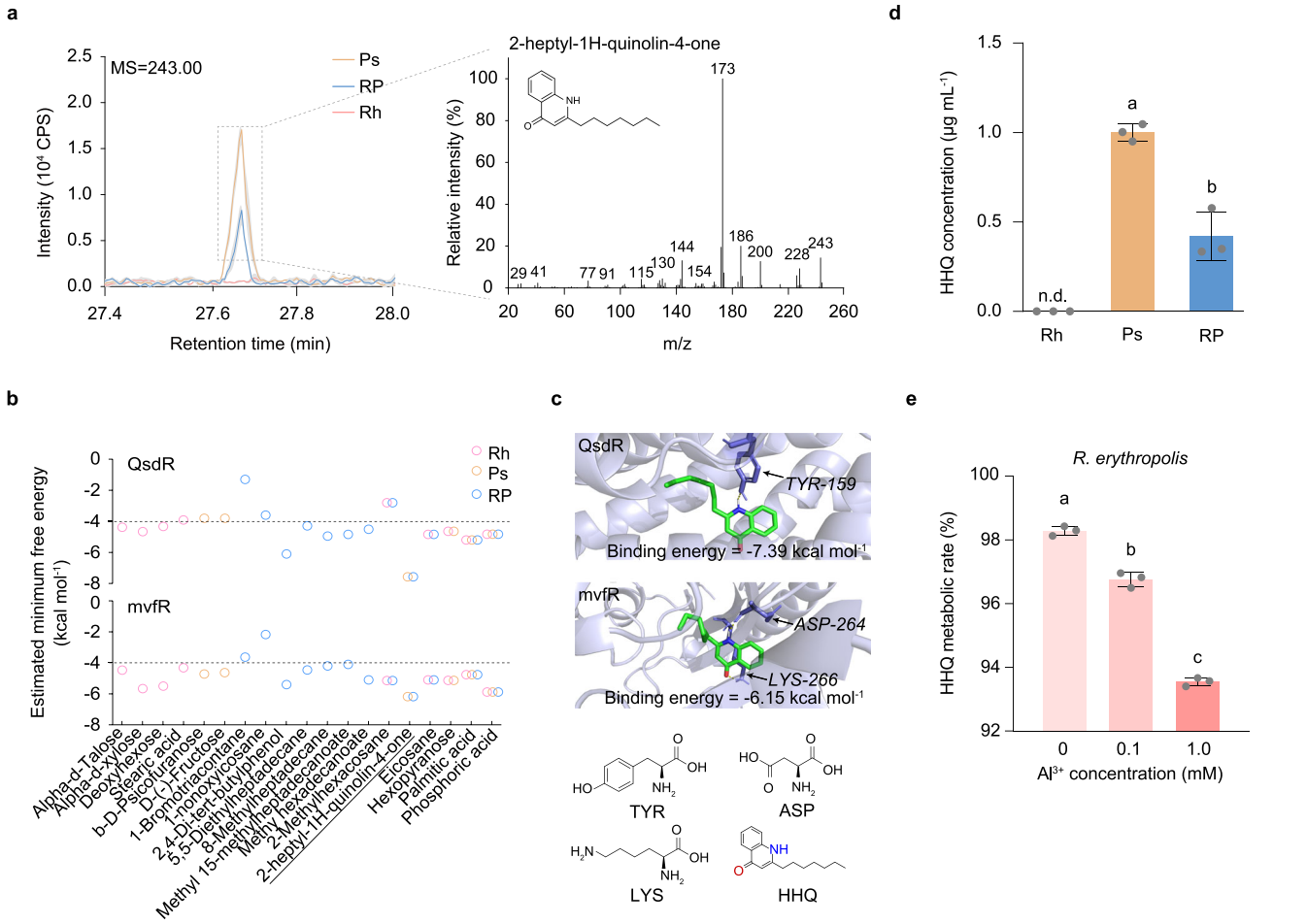

Fig. 2 | Identification, recognition, and fate analysis of the key metabolic substance HHQ. a The primary and secondary spectra of HHQ identified by a single quadrupole gas chromatography–mass spectrometry (GC–MS) system under mono-culture or co-culture conditions. The solid centerline represents the average observed peak, and the shaded area represents the standard deviation ($n = 3$ biological replicates). **b** The predicted minimum binding free energy of 19 substances detected with protein molecules via flexible docking. The dashed line at −4 represents the threshold of binding free energy for ligand binding to receptor proteins. **c** The binding site corresponding to the minimum free energy generated by the combination of HHQ and protein. TYR tyrosine, ASP aspartic acid, LYS lysine. **d** Determination of the relative concentration of HHQ in the culture media of mono-cultures or co-cultures of *R. erythropolis* and *P. aeruginos*. **e** The degradation rate of *R. erythropolis* to 20 μM HHQ at different Al^{3+} concentrations (pH 4.0) after 8 h of incubation. In (**d**, **e**), bars represent the mean ± s.d. ($n = 3$ biological replicates). Different letters indicate significant differences ($P < 0.05$, one-way ANOVA, two-sided Fisher's LSD test). Rh mono-culture of *R. erythropolis*, Ps Rh: mono-culture of *P. aeruginosa*, RP co-culture of *R. erythropolis* and *P. aeruginosa*. Source data are provided as a Source Data file.

P. aeruginosa and *R. erythropolis* (fold change > 1.5, FDR < 0.05). In mono-cultured *P. aeruginosa* exposed to Al stress, downregulated DEGs were predominantly associated with flagella assembly, chemotaxis, and biofilm formation pathways (Supplementary Fig. 9a). Upon co-culture with *R. erythropolis*, the downregulated DEGs in *P. aeruginosa* were mainly enriched in pathways related to two component system, QS, and amino acid metabolism (Supplementary Fig. 9b).

Furthermore, *R. erythropolis* revealed distinct expression patterns in the cell wall synthesis and tryptophan metabolism pathways under different conditions. In the mono-cultures, these pathways were significantly repressed under Al stress, as characterized by an enrichment of downregulated DEGs (Supplementary Fig. 9c). Conversely, in co-culture, these pathways were markedly upregulated (Supplementary Fig. 9d). Network analysis of the top 10 enriched pathways indicated that DEGs associated with the tryptophan metabolism pathway were connected to the peptidoglycan biosynthesis pathway, exclusively through the two-component system pathway (Supplementary Fig. 10a, b). It suggested that genes related to tryptophan metabolism contribute to peptidoglycan biosynthesis.

We then examine the cellular morphology and quantify cell wall characteristics by scanning electron microscopy (SEM) and atomic force microscopy (AFM) under Al stress, respectively. Cell wall damage inflicted upon *R. erythropolis* by Al^{3+} stress was ameliorated by both co-culture with *P. aeruginosa* and treatment with 20 μM HHQ in minimal media, as evidenced by the absence of discernible folds or ruptures (Supplementary Fig. 11). As the Al^{3+} concentrations increased from 0 mM to 0.1 mM and 1 mM, the cell wall thickness of *R. erythropolis* thinned from 8.56 nm to 4.10 nm and 3.34 nm, respectively (Supplementary Fig. 12). Concurrently, the wall roughness decreased from 6.36 nm (0 mM Al^{3+}) to 4.11 nm (1 mM Al^{3+}) (Fig. 3a). The detrimental effects of Al on cell wall thickness and roughness were mitigated by the addition of 20 μM HHQ. Specifically, the cell wall thickness of *R. erythropolis* increased to 11.20, 14.89, and 19.34 nm, respectively (Supplementary Fig. 12), and the wall roughness increased from 5.93 (0 mM Al^{3+}) nm to 8.52 nm (1 mM Al^{3+}) (Fig. 3b). For *P. aeruginosa* under increased Al concentrations, the cell thickness significantly increased, while the wall roughness remained merely change (Fig. 3c).

We established a potential pathway for *R. erythropolis* to degrade quinolone compound HHQ, synthetic tryptophan, and promote the synthesis of cell wall-related substances (Supplementary Fig. 13). The expression levels of key genes involved in cell wall synthesis and quinolone oxidation were quantified using qRT–PCR. Our findings

https://doi.org/10.1038/s41467-024-54616-0

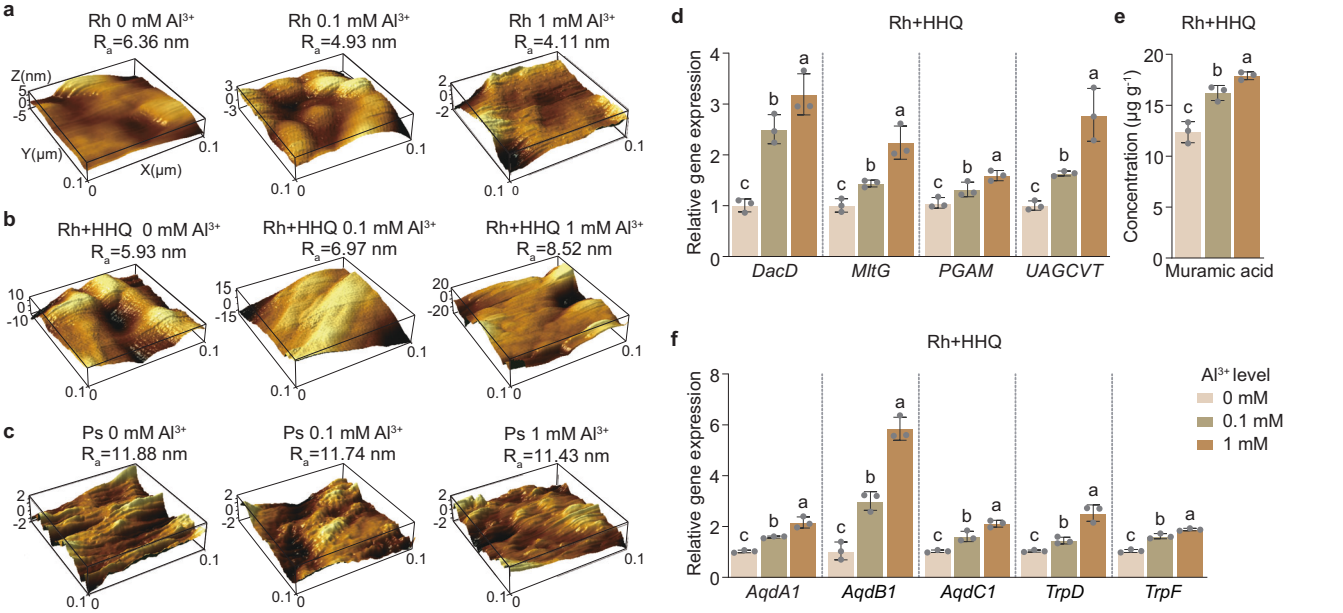

Fig. 3 | *R. erythropolis* strengthens cell wall synthesis by metabolizing HHQ. **a**–**c**, 3D results of cell wall thickness and wrinkle degree among different treatments. **d** Analysis of the relative expression levels of cell wall acid synthesis-related genes (*DacD*, *MltG*, *PGAM*, and *UAGCVT*) in *R. erythropolis* under different concentrations of added Al^{3+} (pH 4.0) with the addition of 20 μM HHQ. **e** Measurement results of the cell wall acid concentration in *R. erythropolis* with the addition of HHQ at different Al^{3+} concentrations (pH 4.0). **f** Analysis of the relative expression levels of alkylquinolone-specific catabolic enzymes (*AqdA1*, *B1*, *C1*) and ribosome transferase genes (*TrpD*, *F*) in *R. erythropolis* treated with different concentrations of Al^{3+} (pH 4.0) and supplemented with 20 μM HHQ. In (**d**–**f**), bars represent the mean ± s.d. ($n = 3$ biological replicates). Different letters indicate significant differences ($P < 0.05$, one-way ANOVA, two-sided Fisher's LSD test). R_a roughness rate; Rh mono-culture of *R. erythropolis*, Rh+HHQ mono-culture of *R. erythropolis* with the addition of HHQ, Ps mono-culture of *P. aeruginosa*. Source data are provided as a Source Data file.

revealed that the key genes of cell wall synthesis pathways (*DacD*, *MltG*, *PGAM*, and *UAGCVT*) in *R. erythropolis* were significantly downregulated in Al^{3+} gradients (Supplementary Fig. 14), while upregulated in response to increasing Al^{3+} concentrations supplemented with 20 μM HHQ (Fig. 3d). Quantitative analysis revealed that cell wall biosynthesis with the formation of muramic acid in *R. erythropolis* cells increased with Al^{3+} concentration in the presence of HHQ. Muramic acid concentration showed a 1.31-fold increase (16.20 ± 0.74 μg g^{-1} at 0.1 mM Al^{3+}) and a 1.45-fold increase (17.90 ± 0.38 μg g^{-1} at 1 mM Al^{3+}) relative to those without Al stress (Fig. 3e). Additionally, the addition of HHQ increased the expression levels of alkylquinolone-specific catabolic enzymes (*AqdA1*, *B1*, and *C1*) and ribotransferase genes (*TrpD and TrpF*), linking HHQ degradation to tryptophan synthesis (Fig. 3f). Similarly, the bacteria colonization and key gene expression patterns were validated in both sterilized clay-based and acidic soil systems (Supplementary Figs. 15 and 16, Supplementary Note 2). This connection likely facilitates the further synthesis of tryptophan during co-culture, subsequently contributing to cell wall formation.

To elucidate the role of tryptophan in modulating cell wall biosynthesis and bolstering the defense mechanisms of *R. erythropolis* against Al stress, we analysed the transcription levels of genes involved in relevant pathways under a gradient of Al^{3+} concentrations. Our results revealed that Al^{3+} exposure led to a significant downregulation of phosphoglucosamine mutase (*PGAM*) and UDP-*N*-acetylglucosamine 1-carboxyvinyltransferase (*UAGCVT*) genes, which are integral to *N*-acetylmuramic acid production in *R. erythropolis*. The provision of exogenous tryptophan (Rh+Trp) or co-culturing with *P. aeruginosa* substantially enhanced the expression levels of these genes (Fig. 4a). Consistent trends were observed in the transcriptional activity of the D-alanyl-D-alanine carboxypeptidase (*DacD*) and murein endolytic transglycosylase (*MltG*) genes, as well as corresponding changes in the muramic acid concentration (Fig. 4b, Supplementary Fig. 17). The growth kinetics indicated by population density further confirmed the ability of tryptophan to promote the proliferation of *R. erythropolis* under Al stress (Supplementary Fig. 18).

Discussion

Cross-feeding is a widespread phenomenon in natural microbial communities[5]. In our study, we reported that cross-feeding between microbial species with varying Al resistance capabilities strengthens the effectiveness of consortia. In the co-culture system, *P. aeruginosa*, characterized by its robust resistance to Al, initially occupies a stable niche and produces the metabolic substrate HHQ. This compound establishes a unidirectional cross-feeding relationship with *R. erythropolis* (Fig. 5a). Subsequently, *R. erythropolis* degrades HHQ into anthranilic acid (AA), which is then transformed into tryptophan. Tryptophan plays a crucial role in the synthesis of *N*-acetylmuramic acid, ultimately facilitating peptidoglycan biosynthesis (Fig. 5b). Furthermore, the decreased accumulation of HHQ alleviates density-dependent constraints on *P. aeruginosa*, enhancing its metabolic activity. Within the microbial community, these ecological exchanges fortify their collective resistance to Al stress and amplify their communal activities.

Tryptophan, an essential amino acid, plays a crucial role in microbial physiology, including the synthesis of cell wall components such as muramic acid and peptidoglycan[21]. As demonstrated in Fig. 4, Supplementary Figs. 17 and 18, the availability of tryptophan influenced the stability and function of *R. erythropolis*, underscoring the significance of understanding metabolic dependencies in community design. However, tryptophan was undetectable under both mono-culture and co-culture conditions (Supplementary Fig. 19), suggesting that it is unlikely to be the primary cross-feeding metabolite exchanged between microorganisms. This absence could be attributed to suboptimal environmental pressures that compel microbes to shift their strategic focus from maximizing growth yield and resource acquisition to investing in stress tolerance traits[22], thereby altering the composition of metabolic pools shared by other microorganisms[23].

https://doi.org/10.1038/s41467-024-54616-0

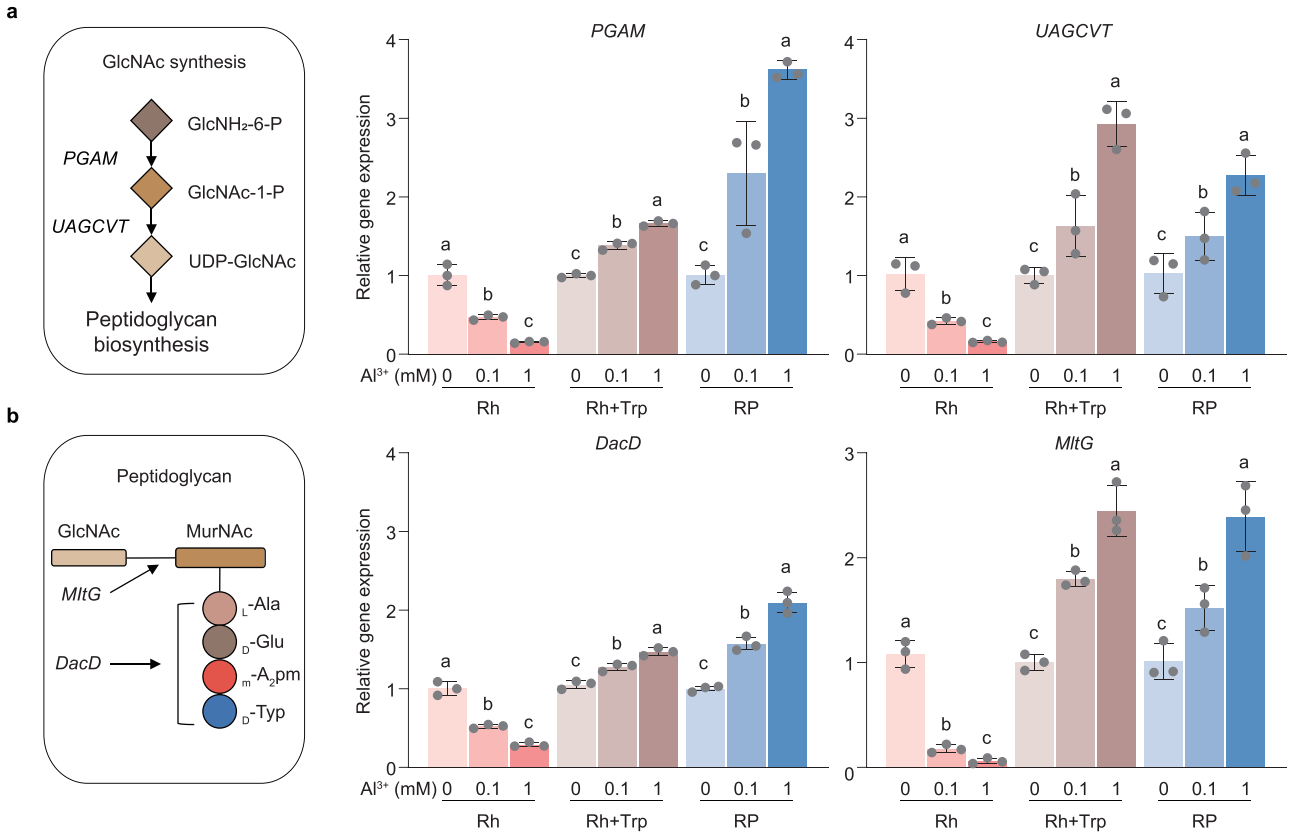

Fig. 4 | Transcriptional expression analysis of tryptophan-mediated genes related to peptidoglycan biosynthesis in *R. erythropolis*. **a** Relative gene expression of functional genes involved in the biosynthesis of *N*-acetylglucosamine (GlcNAc). **b** Relative gene expression of functional genes involved in the biosynthesis of peptidoglycan. In (**a**, **b**), bars represent the mean ± s.d. ($n = 3$ biological replicates). Different letters indicate significant differences ($P < 0.05$, one-way ANOVA, two-sided Fisher's LSD test). Rh mono-culture of *R. erythropolis*, Rh+Trp *R. erythropolis* with the addition of tryptophan, RP co-culture of *R. erythropolis* and *P. aeruginosa*. Source data are provided as a Source Data file.

Dominant species could redirect resources towards fortifying resistance against environmental stresses rather than sharing endogenous metabolites such as amino acids[24]. Therefore, microorganisms with high Al tolerance, when exposed to Al toxicity, drive amino acids to become competitive nutrients to maintain normal cell wall morphology. This was evidenced by the thicken cell walls of Al-resistant *P. aeruginosa* with increasing Al^{3+} concentrations (Supplementary Fig. 12). We discovered that cross-feeding mechanisms mediated by quinoline compounds benefit microorganisms with low Al tolerance, enhancing their performance under Al stress. In summary, these results highlight the complexity of microbial resource allocation and metabolic acclimatization under environmental stress, offering new insights into microbial ecological dynamics.

In engineering SynComs to bolster plant health and growth within agricultural soils, a significant hurdle lies in ensuring that the introduced microbial strains can persist within the indigenous microbial networks[25]. The role of native microbes in surmounting this challenge has been underscored[26], bringing microbial interactions to the fore as one of the important aspects in the orchestration of microbial consortia aimed at eliciting desired outcomes. For example, our findings reveal that the plant growth-promoting effects induced by the SynCom were markedly superior to those achieved through individual inoculations (Supplementary Figs. 1 and 2). This enhancement can be ascribed to an elevation in both the abundance and metabolic activity of *P. aeruginosa* and *R. erythropolis* (Fig. 1a, d). *P. aeruginosa*, through QS mechanisms, produces antibiotics that facilitate its colonization, while *R. erythropolis* degrades HHQ, culminating in a synergistic co-colonization in acidic soils. Similarly, SynComs designed based on these microbial interactions exhibit augmented production of protective metabolites and an extended community longevity[27]. Therefore, leveraging cross-feeding and QS systems in natural environments can aid in the design of microbial consortia that may have competitive advantages over mono-cultures in terms of productivity, resource allocation and utilization, metabolic complexity, and invasion resistance[6,28].

In summary, our study revealed that *R. erythropolis* augments its metabolic activity by harnessing the quinolone metabolites excreted by *P. aeruginosa*. This increase in tryptophan production subsequently modulates the peptidoglycan synthesis pathway, leading to cell wall reinforcement and an enhanced capacity for Al tolerance. Additionally, the efficient catabolism of these compounds by *R. erythropolis* mitigates the density-dependent constraints typically imposed by QS in *P. aeruginosa* populations. These findings offer empirical support for the natural tendency of microorganisms to establish mutualistic partnerships, particularly in hostile environments such as acidic soils with Al toxicity. The uncovered interplay between *R. erythropolis* and *P. aeruginosa* not only illuminates the intricate web of microbial interactions but also has implications for fields ranging from environmental microbiology to biotechnological applications. By deciphering the metabolic dialog between these species, we can build a foundation for programming innovative strategies to enhance microbial fitness and resilience in natural and engineered systems in the future.

Methods

Bacterial growth conditions

The bacterial species used in this study, *R. erythropolis* and *P. aeruginosa*, were isolated from the rhizosphere soil of *japonica* rice, Nanjing46, grown in acidic red soil. *R. erythropolis* and *P. aeruginosa* were

https://doi.org/10.1038/s41467-024-54616-0

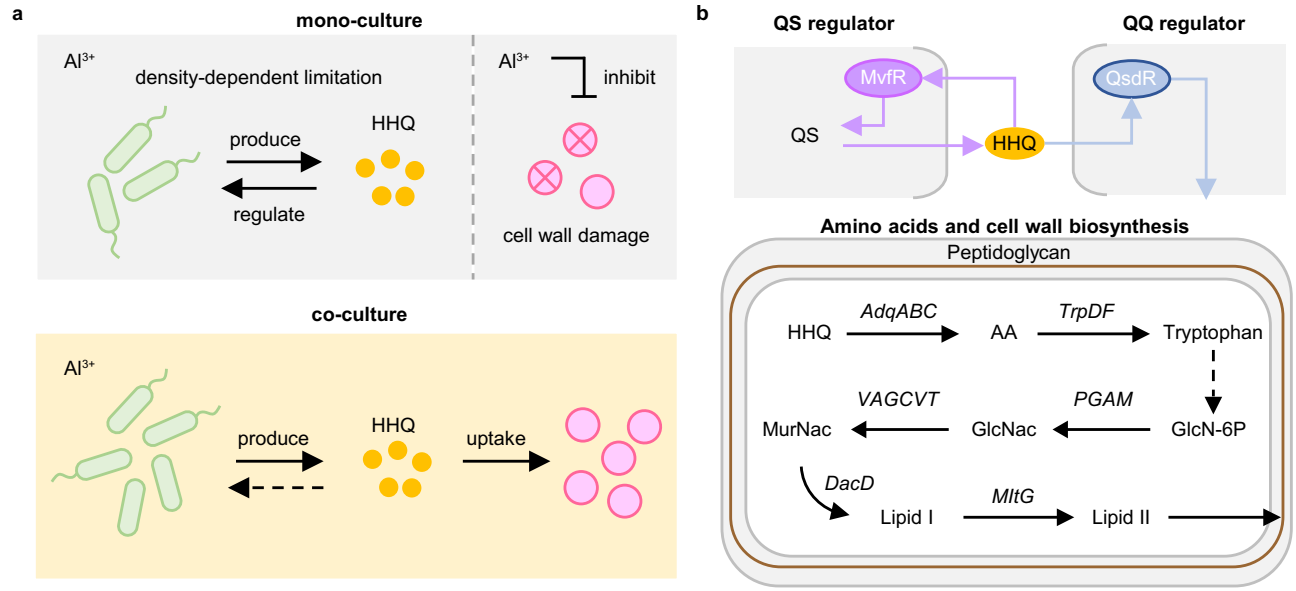

Fig. 5 | Cooperative coexistence mechanism of *R. erythropolis* and *P. aeruginosa* to improve Al-tolerance based on cross-feeding of HHQ. a In mono-culture, *P. aeruginosa*, which demonstrates greater Al resistance, experiences density-dependent limitation through the production and regulation of the quorum sensing molecule, HHQ. Conversely, the mono-culture of *R. erythropolis* was inhibited by the presence of Al^{3+}, leading to cell wall damage. When *R. erythropolis* and *P. aeruginosa* are co-cultured, HHQ, released by the producer *P. aeruginosa*, is taken up by the consumer *R. erythropolis*. This uptake mitigates the self-limiting growth of *P. aeruginosa*, resulting in improved interspecies interaction and enhanced communal resistance to Al^{3+} toxicity. **b** HHQ is synthesized by *P. aeruginosa* under the regulation of the transcription factor MvfR, resulting in self-limiting by quorum sensing. *R. erythropolis* can metabolize HHQ, inducing the expression of its own QsdR transcription factor, and activating the expression and synthesis of downstream oxidative enzymes (*AqdABC*). During this process, HHQ is cleaved and oxidized to form anthranilic acid (AA), which is subsequently converted into tryptophan by riboflavin transferase (*TrpDF*). Tryptophan then induces the regulation of *PGAM* and *UAGCVT* genes involved in the synthesis of *N*-acetylglucosamine (GlcNAc) and acetyl muramic acid (MurNac) in *R. erythropolis*, further activating the regulatory genes *DacD* and *MltG* for lipid I and II synthesis, thereby facilitating cell wall biosynthesis.

shaken overnight (28 °C, 180 rpm) using Luria–Bertani (LB) media (5 g L^{-1} yeast extract, 10 g L^{-1} tryptone, 10 g L^{-1} sodium chloride). When the optical density at 600 nm (OD_{600}) reached 0.6–0.8 during the exponential growth phase, single colonies were isolated by streaking on plates into a pure culture. These colonies were then used for subsequent culture experiments.

For further observations and analysis, minimal media and modified minimal media (MM) supplemented with different forms of P were used. The minimal media was composed of 2 g L^{-1} $(NH_4)_2SO_4$, 1.2 mM $K_2HPO_4 \cdot 3H_2O$, 0.8 mM KH_2PO_4, 1 g L^{-1} trisodium citrate, 80 nM $MnCl_2 \cdot 4H_2O$, 1 µM $FeSO_4 \cdot 7H_2O$, 0.5 mM $MgSO_4 \cdot 7H_2O$, and 2% D-glucose. The MM included 0.5 g L^{-1} $(NH_4)_2SO_4$, 0.3 g L^{-1} KCl, 0.3 g L^{-1} NaCl, 0.03 g L^{-1} $MnSO_4 \cdot H_2O$, 0.03 g L^{-1} $FeSO_4 \cdot 7H_2O$, and 0.03 g L^{-1} $MgSO_4 \cdot 7H_2O$, supplemented with 1 g L^{-1} sodium phytate or 1 g L^{-1} tricalcium phosphate as the sole P source, respectively (Supplementary Method 1 and 2). Note that the Al stress conditions in this study were established by addition of $AlCl_3$ to the culture medium, with the specified concentrations referring to the added concentrations of Al^{3+}. $AlCl_3$ was filtered through a 0.22 µm filter for sterilization before being added to the media with a final pH of 4.0. This approach to establishing Al stress environment has been validated in previous studies[18,29].

Synthetic microbial community preparation for inoculation

Individual colonies of *R. erythropolis* and *P. aeruginosa* were inoculated into 50 mL of liquid LB media and incubated at 28 °C with shaking at 180 rpm for 24 h, reaching a density of ~2.3×10^8 CFU mL^{-1}. Then, the two strains were propagated in a fermentation tank for 18 h. The resultant bacteria biomass was harvested using a disk centrifuge method (10,000 × *g*, 5 min) to remove any residual LB medium. The SynCom formulations consisted of an equimolar mixture of the strains suspended in ultrapure water with a final concentration of 1×10^8 CFU mL^{-1}. Three days following the transplantation of rice seedlings, each plant was treated with 25 mL of the SynCom solution.

Experimental site description and field experiments

The field experiment was established at the Yingtan National Agricultural Ecosystem Observation and Research Station in Jiangxi Province (28°12′N, 116°55′E), China. The experimental area has a typical subtropical climate with an average annual precipitation of 1881.8 mm and an average annual temperature of 18.4 °C. The field soil used in the experiment was Quaternary red clay with a soil content of 36%, which is strongly weathered and has high Al and iron oxide contents. It is classified as a typical Plinthosol by the US soil classification system, and its relevant physical and chemical properties are shown in Supplementary Data 2. In accordance with local traditional farming methods, the experimental field was managed using a single rice crop system per year, employing furrow irrigation and consistent weed management throughout the growing season.

Rice seeds from *japonica* Nanjing 46 were surface sterilized in 75% ethanol for 30 s and 2.5% sodium hypochlorite three times for 15 min and germinated on Murashige and Skoog (MS) agar media for 15 days (25 °C). Rice plants in similar growth stages were subsequently transplanted into field plots, with 40 plants per plot. The size of each plot was 1.5 m × 6.0 m, with furrows serving as boundaries. The field experiment included four treatments: non-inoculation (CK), mono-inoculation with *R. erythropolis* (Rh), mono-inoculation with *P. aeruginosa* (Ps), and inoculation with co-cultured *R. erythropolis* and *P. aeruginosa* (RP), with each treatment having one plot (Supplementary Fig. 1). During the heading and maturity stages of rice, photos were taken using a digital camera (RICH GRIII, R02010, Vietnam), and the leaf chlorophyll content (SPAD-502-plus, Konica Minolta, Japan) and rice plant height were measured. A total of 40 rice plants were

harvested at 110 days after transplanting. Shoot biomass and panicle weight per plant were measured.

Pot experiments

The soil used for the pot experiment was collected from the field site. The soil was sieved through a 10-mesh screen to remove stones and impurities. A total of 145.6 g of red soil was transferred to a 160 mL root box and compacted to ensure a bulk density of 1.3 for each root box. Surface-sterilized rice seedlings from Nanjing46 were transplanted with one plant per root box. The pot experiment included four treatments: non-inoculation, mono- and co-cultures of *R. erythropolis* and *P. aeruginosa*. Each treatment was replicated five times. The leaf chlorophyll content and rice plant height were assessed at seven-day intervals while documenting the growth status of the plants. At maturity, shoot and grain samples were collected from the rice plants. The roots were shaken to remove loosely adherent soil, followed by collection of adhering soil (rhizosphere soil) from the root surface[30]. Root samples were dried to a constant weight in an oven at 65 °C and then Al concentration in rice roots was measured (Supplementary Method 3). Soil samples were immediately stored in a −80 °C freezer for subsequent determination of the absolute abundance of 16S rRNA genes.

Reverse-Raman-D_2O for assessing the bacterial metabolic activity

Reverse-Raman-D_2O was used to measure the metabolic activity of the bacteria[31]. In brief, single strains of *R. erythropolis* and *P. aeruginosa* and their co-cultures were initially cultured in LB media supplemented with 50% heavy water (99.9 atomic% D, CIL, Inc., USA) for 24 h in triplicate. After labeling the cells with heavy atoms D, the cultures were transferred to minimal media without D_2O. Different concentrations of $AlCl_3$ (0, 0.1, and 1 mM, pH 4.0) were added under sterile conditions. The cultures were then incubated at 28 °C and 180 rpm for 5 h. Cells were harvested by centrifugation (13,600 × *g*, 10 min) at room temperature, washed twice with ultrapure water, and resuspended in deionized water to disperse cell clusters.

For Raman measurement, 2 µL of cell suspension was loaded on Al foil and air-dried. Raman spectra were acquired using a LabRAM HR Evolution microscope (HORIBA Scientific, France) with a 532 nm Nd:YAG laser (laser Quantum), a 100× objective lens (Olympus, NA = 0.9), and a spectral range of 400–3200 cm^{-1}. A total of 30 individual bacteria were randomly selected from each treatment for Raman measurement. Baseline correction, normalization, and subsequent Fourier transformation were consistently performed on all measurements using LabSpec6 software (Horiba Jobin-Yvon). The $C–D_{ratio}$ was calculated to assess D assimilation, using the integral intensity of the C–H peak (2800–3100 cm^{-1}) and C–D peak (2040–2300 cm^{-1}), with lower $C–D_{ratio}$ indicating higher metabolic activity under Al stress. In co-culture, the resonance Raman peak of cytochrome C (heme group, 749.95 cm^{-1}) was selected as the basis for distinguishing between *P. aeruginosa* and *R. erythropolis*[32].

FISH labeling of *R. erythropolis*

The fresh rhizosphere soil samples were fixed with 320 µL of a 25% (w/v) particle-free paraformaldehyde solution (4% final concentration) supplemented with 1× phosphate-buffered saline (PBS). The mixed suspension was subsequently fixed at 4 °C for 5 h, washed twice with 1× PBS, centrifuged at 10,000 × *g* for 5 min at 4 °C, and stored in PBS/ethanol (1:1) at −20 °C for further processing. Then, 100 µL of the stored sample was diluted with 900 µL of PBS/ethanol and dispersed by ultrasonication for 30 s.

Subsequently, 30 µL of the dispersed sample was mixed with 60 µL of 1× PBS, 10 µL of 0.01% SDS (w/v) and 10 µL of 1% (w/v) low melting point agarose at 55 °C. 10 µL of the sample suspension was pipetted onto epoxy-coated glass slides (Thermo Fisher Scientific, Wilmington, USA). The slides were dried in an incubator at 37 °C and dehydrated using a graded series of ethanol (50% for 5 min, 80% for 1 min, and 98% for 1 min). For permeabilization of the cell walls, each well of the slides with agarose-embedded samples was treated with 10 µL of a lysozyme solution (10 mg of lysozyme, 100 µL of 0.5 M EDTA (pH 8.0), 100 µL of 1 M Tris–HCl (pH 8.0), and 800 µL of ultrapure H_2O). After incubation in a humidified PE tube (50 mL) for 1 h at 37 °C, the slides were washed using ultrapure water, and dehydrated. Endogenous peroxidase activity was inactivated by the addition of 0.15% H_2O_2 in methanol.

For in situ labeling, an oligonucleotide probe (sequence: 5′-CY3-CACCTGCCAGAAAATCCTTGGATCAACTG-3′) was used of *R. erythropolis* bacteria[33]. The hybridization buffer was set to a formamide concentration of 55% (0.9 M NaCl, 20 mM Tris–HCl (pH 8.0), 10% (w/v) dextran sulfate, 2% (w/v) blocking reagent (Roche, Mannheim, Germany), 0.1% (w/v) sodium dodecyl sulfate, and 55% (v/v) formamide). Hybridization was performed at 37 °C for 2 h, followed by washing in prewarmed buffer. The slides were transferred to a tube containing 50 mL of prewarmed washing buffer (3 mM NaCl, 5 mM EDTA (pH 8.0), 20 mM Tris–HCl (pH 8.0), and 0.01% (w/v) SDS). The slides were then treated with 0.05% (v/v) Triton X-100 (Solarbio Science & Technology Co., Ltd, Beijing, China)-amended PBS for 15 min at room temperature, rinsed with ultrapure water, and dehydrated with ethanol.

Finally, 10 µL of 4,6-diamido-2-phenylindole (DAPI) was added to each well and incubated for 8 min in the dark. The labeled sections were observed using a fluorescence microscope (Nikon Ti-S, Nikon Co., Ltd, Tokyo, Japan) with excitation at 510–560 nm and emission at 590 nm. Twenty different regions were collected from each sample and probe, with more than 1000 cells per region.

Soil DNA extraction

Soil DNA was extracted using a previously described method[34]. Briefly, extractions were performed from 0.5 g of well-mixed soil from each sample by combining freeze grinding and sodium dodecyl sulfate for cell lysis. The crude DNA was further purified by agarose gel electrophoresis, followed by consecutive extractions with phenol, chloroform, and butanol. The quality of the extracted DNA was assessed based on the absorbance ratio at 260/280 nm and 260/230 nm using a Nanodrop 2000 (Thermo Fisher Scientific, Wilmington, DE, USA) and a Qubit 3.0 spectrophotometer (Thermo Fisher Scientific, USA). All DNA samples were stored at −80 °C.

Absolute quantification of *R. erythropolis*, *P. aeruginosa*, and rhizosphere bacteria in soil

qRT–PCR was performed in a volume of 20 µL, which contained 10 µL of 2× SG Fast qPCR Master Mix (Sangon Biotech Co., Ltd, Shanghai, China), 0.4 µL of 10 µM forward and reverse primers, and 2 µL of template DNA diluted in 7.2 µL of enzyme-free water[35]. The qRT–PCR primers were designed and assessed using Primer Premier 6.00 (Premier Biosoft) software with a melting temperature of 80 ± 5 °C. The primer pairs used for each gene are detailed in Supplementary Data 3. The amplified DNA fragments ranged in size from 100 to 300 bp. Using an external standard method, quantitative data were analysed using StepOne software (version 2.3, Applied Biosystems, CA, USA). The abundances of *R. erythropolis*, *P. aeruginosa*, and total soil bacteria were calculated as the average fold difference between the samples and the respective 10-fold serial dilutions of plasmid standards in their respective standards[36]. The bacterial 16S rRNA gene copies number calculated in this study had been adjusted using the rrnDB database (https://rrndb.umms.med.umich.edu/)[37]. The bacterial abundance is expressed as the number of gene copies per gram of soil.

Inference of potential metabolic pathways for HHQ

Based on previous literature, we established a potential metabolic pathway for *R. erythropolis* to degrade the quinolone compound HHQ,

which involves multiple steps and a series of enzymes, including quinolone monooxygenase, dioxygenase hydrolase, carboxylesterase, and ribotransferase (Supplementary Fig. 7). Among them, alkylquinolone-specific catabolic enzymes (*AqdB1*, *AqdC1*, and *AqdA1*) are key genes involved in the synthesis of the tryptophan precursor AA[38]. Ribotransferase genes (*TrpD* and *TrpF*) participate in the subsequent biosynthesis of tryptophan[39]. At the same time, tryptophan or its derivatives play an important role in the synthesis of microbial cell walls, especially peptidoglycan[40]. The main skeleton structure of the cell wall peptidoglycan is formed by the polymerization of amino sugars and muramic acid[41]. The key functional genes *PGAM* and *UAGCVT* participate in the synthesis of *N*-acetylmuramic acid[42]. *N*-acetylmuramic acid and *N*-acetylglucosamine are linked by β-1,4 glycosidic bonds under the regulation of *MltG*, and *DacD* can regulate the composition of oligopeptide chains to form a tetrapeptide tail and further bind to form a peptide bridge structure, making peptidoglycan have a mesh structure[43]. The cell wall formed by the aggregation of peptidoglycan is crucial for maintaining the normal physiological functions and structural integrity of cells under Al stress[44].

Relative quantification of functional genes in *R. erythropolis*

Nine functional genes and the housekeeping gene *gyrB*, were identified to elucidate the impact of tryptophan and HHQ on the metabolism of quinolone substances, tryptophan production, peptidoglycan synthesis, and cell wall peptidoglycan crosslinking in *R. erythropolis*. The sequences of the primers used for amplification of related genes are listed in Supplementary Data 3. The results of primer specificity validation are provided in Supplementary Figs. 20–23 and Supplementary Data 4. The nucleotide sequences are presented in Supplementary Data 5.

Four experimental groups are included: Rh, RP, a mono-culture of *R. erythropolis* supplemented with tryptopha (Rh+Trp), and a mono-culture of *R. erythropolis* supplemented with HHQ (Rh+HHQ). These groups were cultivated in minimal media supplemented with 0, 0.1, and 1 mM $AlCl_3$, with three replicates for each group at 28 °C and 180 rpm for 24 h. After incubation, the bacterial solution was centrifuged at 13,400 × *g* and 25 °C, and the cell precipitates were washed in 100 µL cold TE buffer (10 mM Tris-HCl, 1 mM EDTA, pH 8.0) and stored at −80 °C.

Total RNA extraction, reverse transcription, and qRT–PCR were performed using previously reported methods[38]. Briefly, the cell suspension was thawed and resuspended in 1 mL of TE buffer containing 3 mg mL^{-1} lysozyme for 15 min. Total RNA was extracted using the RNAprep Pure Cell/Bacteria Kit (TIANGEN Biotech Co., Ltd, Beijing, China). The remaining DNA impurities were digested with 80 µL of DNase I without RNA, and then, 1 µg of sample RNA was used to synthesize first-strand DNA at 42 °C through a FastKing RT kit (TIANGEN Biotech Co., Ltd, Beijing, China). The fold change in target gene expression was analysed by the comparative threshold cycle (*CT*) method[45]. The calculation formula is:

$$2^{-\Delta\Delta CT} = 2^{-\left[\left(CT_{\text{gene of interest}} - CT_{\text{gyrB}}\right)_{\text{smpleA}} - \left(CT_{\text{gene of interest}} - CT_{\text{gyeB}}\right)_{\text{smpleB}}\right]} \quad (1)$$

where sample A is the cDNA sample from each treatment group, and sample B is the control group. The amplification efficiency of each primer was detected using LinRegPCR (version 2013.1, Amsterdam, Netherlands).

Prokaryotic chain-specific RNA-seq analysis

R. erythropolis and *P. aeruginosa* strains were cultured individually or co-cultured in minimal media supplemented with 0 and 0.1 mM $AlCl_3$ (pH 4.0) for 24 h. Three parallel experiments were conducted for each group. After incubation, the cell suspensions were collected by centrifugation at 13,400 × *g* for 5 min, and all the samples were immediately transferred to −80 °C for total RNA extraction. The supernatants were passed through a 0.22 µm filter membrane, and 1 mL of each liquid was stored at −20 °C for metabolite identification. Total RNA was extracted from each sample using TRIzol reagent (Merck KGaA, Darmstadt, Germany) according to the manufacturer's instructions.

The quality of the extracted RNA was assessed using a Nanodrop 2000 (Thermo Fisher Scientific, Wilmington, USA) and an Agilent 4200 Tape Station bioanalyzer (Agilent Technologies, CA, USA). Only RNA samples with an RNA integrity value (RIN) ≥ 7 were selected for cDNA library construction. The quality-controlled RNA samples were further processed by using a Ribo-Zero rRNA removal kit (Bacteria; Epicenter, WI, USA). First-strand cDNA was synthesized using random hexamers, followed by RNA strand degradation using RNase H. Second-strand cDNA was synthesized using DNA polymerase I and dNTPs. The remaining overhangs were converted to blunt ends by exonuclease/polymerase activity, and enzymes were removed using the NEBNext Ultra IITM directional RNA library Prep Kit for Illumina. The 3′ ends of the DNA fragments were adenylated, and Illumina PE adapter oligonucleotides were ligated for hybridization.

The cDNA library fragments were purified using the AMPure XP system (Beckman Coulter, Beverly, USA) to ensure a preferred length of 400–500 bp. The number of PCR cycles was adjusted to 15, and the final amplified library was quality checked using a Bioanalyzer 2100 system (Agilent Technologies, CA, USA). An equimolar library was constructed using the Kapa-sybr FAST qPCR Kit Light Cycler 480 (KK4610) and a reference standard from Kapa Biosystems. Each library was sequenced in paired-end mode using the TruSeq SBS kit v3-HS with a read length of 2 × 76 bp on the HiSeq2000 instrument (Illumina) according to the manufacturer's protocol for mRNA sequencing experiments.

The *R. erythropolis* and *P. aeruginosa* genomes (GenBank assembly accession numbers: GCA_001715845.1 and GCA_016743035.1) were used as the reference genome. FastQC was used to evaluate the quality of the RNA sequencing reads. The raw data in Fastq format were preprocessed using sickle (version 1.2) by removing adapter sequences, poly-N, and low-quality reads to obtain clean data[46]. The expression levels of transcripts and genes were calculated based on the expected fragments per kilobase per million reads (FPKM) model of exons. Differentially expressed mRNAs were detected using DESeq (v1.30.0), defined as transcripts with a fold change > 1.5 and a FDR < 0.05. *P*-values were calculated using a negative binomial distribution and corrected for multiple testing by Benjamini–Hochberg (B&H). Weighted gene co-expression network analysis (WGCNA)[47] was performed using the "clusterProfiler" package in R software 4.0.5. Note that the cell wall components pathway includes peptidoglycan (ko00550), arabinogalactan (ko00572), and lipopolysaccharide (ko00571) biosynthesis pathway. Network analysis and visualization were carried out using Gephi software (version 0.9.2).

Metabolite assays

The metabolic compounds produced by *R. erythropolis* and *P. aeruginosa* in mono-cultures and co-culture were identified using a single quadrupole GC–MS system. The bacteria were cultivated in minimal media supplemented with 0 or 0.1 mM $AlCl_3$ (pH 4.0) for 24 h in triplicate. After incubation, the cell suspensions were collected by centrifugation at 13,400 × *g*. The supernatants were transferred evenly to 2 mL Eppendorf centrifuge tubes. Then, 0.5 mL of 3:1 (v/v) methanol:water was added to each tube, and the mixture was vortexed. Quality control samples were prepared with equal volumes of minimum medium. Subsequently, the supernatants were centrifuged at 12,000 × *g* for 15 min at 4 °C, and 350 µL was transferred to glass sampling bottles. After adding 50 µL of BSTFA (containing 1% TMCS), derivatization was carried out for 60 min at 70 °C. The derivatized sample was dried under nitrogen, reconstituted in 500 µL of hexane

(chromatographically pure), filtered through a 0.22 μm membrane, and stored at 4 °C.

The derivatives were analysed on an Agilent 7890B gas chromatography system coupled with an Agilent 5977 A single quadrupole system (Agilent Technologies Inc., CA, USA). The separation of the derivatives was performed using a DB-5 MS fused silica capillary column (30 m × 0.25 mm × 0.25 μm, Agilent JW Scientific, Folsom, CA, USA). The injector temperature was maintained at 250 °C, and a sample volume of 1 μL was injected in splitless mode. The following GC temperature program was used: the initial temperature was set to 80 °C and held for 1 min, then increased at a rate of 5 °C min^{-1} over 40 min to 280 °C, held for 10 min at 280 °C, and finally decreased to 80 °C and held for 2 min. The temperatures of the ion source and connector MS were set to 200 °C and 285 °C, respectively. Mass spectra data were acquired in Q3 scan mode (*m/z* 45–800) with a solvent delay time of 2.5 min. The raw GC–MS data (D format) were converted to a general format (CDF format) using ChemStation analysis software (version E.02.1431, Agilent, CA, USA). Then, the preprocessed data were analysed using Chroma TOF (version 4.34, LECO, St Joseph, MI, USA). The metabolites were characterized using the National Institute of Standards and Technology (NIST) database.

Production and degradation of HHQ

To examine the production of HHQ by *P. aeruginosa* and its degradation by *R. erythropolis* under both aqueous culture and soil conditions, five experiments were conducted. In summary, water-based experiments included: (1) mono- and co-cultures of *R. erythropolis* and *P. aeruginosa* in minimal media supplemented with 0.1 mM $AlCl_3$ (pH 4.0); (2) mono-culture of *R. erythropolis* and mono-culture with an initial concentration of 20 μM HHQ in minimal media, supplemented with 0, 0.1, and 1 mM $AlCl_3$ (pH 4.0); (3–5) pot experiments in natural and sterilized acidic soil, as well as in a sterilized clay-based system, with the following treatments: non-inoculation, mono- and co-cultures of *R. erythropolis* and *P. aeruginosa*, inoculation with *R. erythropolis* and 20 μg L^{-1} HHQ. Additionally, an initial HHQ concentration of 20 μg L^{-1} was established to mimic natural soil levels in sterilized conditions.

In experiment 1 and 2, each group was conducted in triplicate, incubated at 28 °C and 180 rpm for 24 h. The bacterial solution was centrifuged at 13,400 × *g*. The HHQ concentration was determined using a relative quantification method (Supplementary Method 4). For pot experiment 3–5, three replicates were also maintained, and the HHQ concentration was measured using an absolute quantification method (Supplementary Method 5).

Muramic acid concentration in *R. erythropolis*

The experimental groups included mono-culture of *R. erythropolis*, co-culture of *R. erythropolis* and *P. aeruginosa*, mono-culture of *R. erythropolis* supplemented with HHQ, and a mono-culture of *R. erythropolis* supplemented with tryptophan. These groups were cultivated in minimum medium supplemented with 0, 0.1, and 1 mM $AlCl_3$, with three replicates for each group at 28 °C and 180 rpm for 24 h. The cultured bacterial solution was centrifuged for 10 min at 13,600 × *g* to remove the supernatant and obtain the bacterial precipitate.

The bacterial precipitate was dehydrated using a freeze dryer (FreeZone 4.5, Labconco, USA) to obtain a bacterial powder. Subsequently, 0.5 g of bacterial powder was placed in a hydrolysis bottle, and 10 mL of 6 M hydrochloric acid was added and swirled evenly. The mixture was hydrolyzed at 105 °C (in an oven) for 8 h and then vortexed and allowed to stand overnight. 0.5 mL of the supernatant was carefully transferred to a glass test tube, and 100 μL of *N*-methylglucosamine solution (1 mg mL^{-1}) was added as an internal standard. The mixture was dried under a stream of nitrogen, then diluted to 1 mL with methanol for analysis. After filtration through a 0.22 μm membrane, the concentration of muramic acid in the cell wall was detected using an AB 5500 liquid chromatography-tandem mass spectrometry (LC-MS/MS) system (AB SCIEX LLC, MA, USA).

Separation was performed using a Waters Hillc column (100 mm × 2.1 mm, 1.7 μm, Waters, Milford, MA, USA) with a mobile phase consisting of 0.1% formic acid in water (A) and acetonitrile (B) at a flow rate of 0.3 mL min^{-1} and an injection volume of 1 μL. The elution program was as follows: initially 90% phase B was maintained for 0.5 min, then decreased from 90% phase B to 50% within 6.5 min, followed by a maintenance period of 1.5 min. Subsequently, it increased from 50% phase B to 90% within 0.5 min and balanced for 4 min.

The limit of detection limit (LOD) of the instrument was determined by external standards (muramic acid) for quantitative analysis, while internal standard 1 was used for recovery rate and concentration correction of the samples. The mass spectrometry information of the external standard muramic acid was as follows: Q1 = 252.2, Q3 = 126.3, DP = 60 V, and CE = 25 eV (quantification); Q1 = 252.2, Q3 = 216.1, DP = 60 V, and CE = 18 eV (qualitative). The mass spectrometry information of the internal standard *N*-methylglucosamine solution was as follows: Q1 = 196.4, Q3 = 58.2, DP = 70 V, and CE = 25 eV (quantification); Q1 = 196.4, Q3 = 74.1, DP = 70 V, and CE = 25 eV (qualitative). The method LOD refers to a signal peak that is three times greater than the background noise of the instrument. In this study, the LOD of muramic acid was 0.1 μg g^{-1}, and the recovery rate was 82.55%–102%.

Simulation of semiflexible molecular docking of the detected substance

QsdR is the only key transcription factor found in *R. erythropolis* that can regulate quorum-quenching (QQ)-lipase, and it can regulate the expression of pyridine ring oxidation-related enzymes in quinolones[20]. MvfR is a typical LysR-type transcriptional regulatory factor in the *P. aeruginosa* strain that can regulate the expression of pqsA-E genes to adjust QS and the expression of multiple virulence factors[19]. We obtained the protein structures of 4ZA6 (QsdR; accession A0A0C2W9F0) and 6b8a (MvfR; accession Q9I4X0) from the UniProt database. The obtained structures were optimized, dehydrated, and hydrogenated using PyMOL 2.5 software (Schrodinger Inc., NY, USA). The 3D structure PDB file of metabolic detection products was generated using ChemDraw 20.0 (PerkinElmer Inc., CT, USA), followed by the semiflexible docking mode[48] between ligands and receptors performed with AutoDockTools 1.5.7 software. Docking simulations were conducted a minimum of 100 times using the genetic algorithm to obtain the predicted binding free energy results. It is generally believed that a binding free energy less than −4 is the threshold for ligand binding to receptor proteins, and the lower the free energy is, the greater the probability of binding. The results of the molecular docking simulation showed that 2-heptyl-1H-quinolin-4-one (HHQ) could form stable hydrogen bonds with the amino acid residue TYR-159 of the QsdR protein, with a binding energy of −7.39 kcal mol^{-1}, and hydrogen bonds with the amino acid residues ASP-264 and LYS-266 of the mvfR protein, with a binding energy of −6.15 kcal mol^{-1}.

Cell wall morphology observation

The experimental groups included mono-cultures of *R. erythropolis* and *P. aeruginosa*, and mono-cultures of *R. erythropolis* supplemented with 20 μg L^{-1} HHQ, cultured in minimal media supplemented with 0, 0.1, and 1 mM $AlCl_3$ (pH 4.0) at 28 °C and 180 rpm for 24 h. After incubation, the bacterial suspensions were centrifuged at room temperature (13,400 × *g*), and the cell pellets were washed in 100 μL of cold TE buffer (10 mM Tris-HCl, 1 mM EDTA, pH 8.0) for AFM and SEM observation.

For AFM observation, the pretreatment method used for the cell samples was described previously[49]. In brief, the cleaned bacterial samples were fixed in 2.5% glutaraldehyde for 4 h, centrifuged at 6000 × *g* for 5 min, after which the glutaraldehyde was removed, and the samples were washed with PBS three times. Then, 50 μL of bacterial

suspension was transferred onto silicon substrates and dried under flowing nitrogen for testing. The TESPA-V2 probes (Bruker) with a standard spring constant of 37 N m^{-1} and resonance frequency in air of 320 kHz were used as imaging probes for AFM experiments in air. High-resolution scanning probe microscopy (MultiMode 8, Bruker, Karlsruhe, Germany) was used to observe the samples in tapping mode, with an average tip sample force of 260–450 pN. The scanning range was set as 100 nm × 100 nm. The thickness and roughness rate (R_a) of each cell wall were determined by height histograms, and the mean values and standard deviations of each group were calculated using paired t tests for data comparison between groups. All 3D images were created using Nanoscope Analysis software.

For SEM observation, bacterial cells were fixed with 10% formaldehyde solution overnight. During the fixation process, the bacterial suspension was shaken constantly to ensure sufficient contact between the formaldehyde solution and the bacterial sample. Then, the samples were centrifuged at 6000 × *g* for 5 min, and the bacterial samples were dehydrated in gradually increasing ethanol solutions (30%, 50%, 70%, 85%, 90%, and 100%). Each bathing step lasted 10 min, and the samples were dried until use in a freeze dryer. The samples were sputter-coated with gold using a JEOL coating machine (JFC-1100E, JEOL Co., Ltd, Japan), vacuum-dried, observed and photographed under 30,000x magnification using a field-emission scanning electron microscopes (Regulus SU8100, Hitachi High-Tech Corporation, Tokyo, Japan).

Statistics and graphics

The normality assumption and equal variance assumption were evaluated using the Kolmogorov–Smirnov test and Levene test, respectively. One-way ANOVA and Tukey's multiple comparison tests were performed using GraphPad Prism 9 (GraphPad Software Inc., CA, USA). Figures were generated using the R 4.2.1 statistical environment (https://cran.r-project.org/), GraphPad Prism 9, OriginLab 2016, and Microsoft PowerPoint (Microsoft Office Home and Student 2019).

Reporting summary

Further information on research design is available in the Nature Portfolio Reporting Summary linked to this article.

Data availability

The raw sequence data presented in this paper have been deposited in the NCBI BioProject database under accession PRJNA1118919. Primers and genes used in this work are provided in Supplementary Data 3–5. Source data are provided with this paper.

Code availability

The code for the "clusterProfiler" package is deposited in Github [https://github.com/mzy492605141/-clusterProfiler-package-.git].

References

1. Hu, J., Amor, D. R., Barbier, M., Bunin, G. & Gore, J. Emergent phases of ecological diversity and dynamics mapped in microcosms. *Science* **378**, 85–89 (2022).
2. Zengler, K. & Zaramela, L. S. The social network of microorganisms—how auxotrophies shape complex communities. *Nat. Rev. Microbiol.* **16**, 383–390 (2018).
3. Bertness, M. D. & Callaway, R. Positive interactions in communities. *Trends Ecol. Evol.* **9**, 191–193, (1994).
4. Fritts, R. K., McCully, A. L. & McKinlay, J. B. Extracellular metabolism sets the table for microbial cross-feeding. *Microbiol. Mol. Biol. Rev.* **85**, 10–1128 (2021).
5. Ona, L. et al. Obligate cross-feeding expands the metabolic niche of bacteria. *Nat. Ecol. Evol.* **5**, 1224–1232 (2021).
6. Karkaria, B. D., Fedorec, A. J. H. & Barnes, C. P. Automated design of synthetic microbial communities. *Nat. Commun.* **12**, 672 (2021).
7. Zeng, X. et al. Quorum sensing-mediated microbial interactions: mechanisms, applications, challenges and perspectives. *Microbiol. Res.* **273**, 127414 (2023).
8. Amarnath, K. et al. Stress-induced metabolic exchanges between complementary bacterial types underly a dynamic mechanism of inter-species stress resistance. *Nat. Commun.* **14**, 3165 (2023).
9. Dal Bello, M., Lee, H., Goyal, A. & Gore, J. Resource–diversity relationships in bacterial communities reflect the network structure of microbial metabolism. *Nat. Ecol. Evol.* **5**, 1424–1434 (2021).
10. Yu, J. et al. Microbial communities form rich extracellular metabolomes that foster metabolic interactions and promote drug tolerance. *Nat. Microbiol.* **7**, 542–555 (2022).
11. Ge, Z. B. et al. Two-tiered mutualism improves survival and competitiveness of cross-feeding soil bacteria. *ISME J.* **17**, 2090–2102 (2023).
12. Kochian, L. V., Pineros, M. A., Liu, J. & Magalhaes, J. V. Plant adaptation to acid soils: the molecular basis for crop aluminum resistance. *Annu Rev. Plant Biol.* **66**, 571–598, (2015).
13. Panda, S. K. & Matsumoto, H. Molecular physiology of aluminum toxicity and tolerance in plants. *Bot. Rev.* **73**, 326–347 (2007).
14. Yaganza, E. S., Rioux, D., Simard, M., Arul, J. & Tweddell, R. J. Ultrastructural alterations of *Erwinia carotovora* subsp. atroseptica caused by treatment with aluminum chloride and sodium metabisulfite. *Appl. Environ. Microbiol.* **70**, 6800–6808 (2004).
15. Xun, W., Shao, J., Shen, Q. & Zhang, R. Rhizosphere microbiome: functional compensatory assembly for plant fitness. *Comput. Struct. Biotechnol. J.* **19**, 5487–5493 (2021).
16. Lian, T. X. et al. High aluminum stress drives different rhizosphere soil enzyme activities and bacterial community structure between aluminum-tolerant and aluminum-sensitive soybean genotypes. *Plant Soil* **440**, 409–425 (2019).
17. D'Souza, G. et al. Ecology and evolution of metabolic cross-feeding interactions in bacteria. *Nat. Prod. Rep.* **35**, 455–488 (2018).
18. Liu, C. et al. Root microbiota confers rice resistance to aluminium toxicity and phosphorus deficiency in acidic soils. *Nat. Food* **4**, 912–924 (2023).
19. Huang, H. et al. An integrated genomic regulatory network of virulence-related transcriptional factors in *Pseudomonas aeruginosa*. *Nat. Commun.* **10**, 2931 (2019).
20. Chane, A. et al. A flavor lactone mimicking AHL quorum-sensing signals exploits the broad affinity of the QsdR regulator to stimulate transcription of the Rhodococcal *qsd* operon involved in quorum-quenching and biocontrol activities. *Front. Microbiol.* **10**, 786 (2019).
21. Typas, A., Banzhaf, M., Gross, C. A. & Vollmer, W. From the regulation of peptidoglycan synthesis to bacterial growth and morphology. *Nat. Rev. Microbiol.* **10**, 123–136 (2011).
22. Malik, A. A. et al. Defining trait-based microbial strategies with consequences for soil carbon cycling under climate change. *ISME J.* **14**, 1–9 (2020).
23. Yu, F., Zhang, W., Hou, X., Li, Y. & Tong, J. How nutrient loads influence microbial-derived carbon accumulation in wetlands: a new insight from microbial metabolic investment strategies. *Environ. Res.* **217**, 114981 (2023).
24. Nikel, P. I. et al. Reconfiguration of metabolic fluxes in *Pseudomonas putida* as a response to sub-lethal oxidative stress. *ISME J.* **15**, 1751–1766 (2021).
25. Kaminsky, L. M., Trexler, R. V., Malik, R. J., Hockett, K. L. & Bell, T. H. The inherent conflicts in developing soil microbial inoculants. *Trends Biotechnol.* **37**, 140–151 (2019).
26. Zhou, Y. et al. Superiority of native soil core microbiomes in supporting plant growth. *Nat. Commun.* **15**, 6599 (2024).
27. Correia-Melo, C. et al. Cell-cell metabolite exchange creates a pro-survival metabolic environment that extends lifespan. *Cell* **186**, 63–79.e21 (2023).

28. Goyal, A., Wang, T., Dubinkina, V. & Maslov, S. Ecology-guided prediction of cross-feeding interactions in the human gut microbiome. *Nat. Commun.* **12**, 1335 (2021).
29. Famoso, A. N. et al. Development of a novel aluminum tolerance phenotyping platform used for comparisons of cereal aluminum tolerance and investigations into rice aluminum tolerance mechanisms. *Plant Physiol.* **153**, 1678–1691 (2010).
30. Edwards, J. et al. Structure, variation, and assembly of the root-associated microbiomes of rice. *Proc. Natl Acad. Sci. USA* **112**, E911–E920 (2015).
31. Li, H. Z. et al. Phenotypic tracking of antibiotic resistance spread via transformation from environment to clinic by reverse D_2O single-cell raman probing. *Anal. Chem.* **92**, 15472–15479 (2020).
32. Kruse, F. et al. A resonance raman marker band characterizes the slow and fast form of cytochrome c oxidase. *J. Am. Chem. Soc.* **143**, 2769–2776 (2021).
33. Jiang, H. L., Maszenan, A. M. & Tay, J. H. Bioaugmentation and coexistence of two functionally similar bacterial strains in aerobic granules. *Appl. Microbiol. Biotechnol.* **75**, 1191–1200 (2007).
34. Zhou, J., Bruns, M. A. & Tiedje, J. M. DNA recovery from soils of diverse composition. *Appl. Environ. Microbiol.* **62**, 316–322 (1996).
35. Bahram, M. et al. Structure and function of the soil microbiome underlying N_2O emissions from global wetlands. *Nat. Commun.* **13**, 1430 (2022).
36. Ruijter, J. M. et al. Amplification efficiency: linking baseline and bias in the analysis of quantitative PCR data. *Nucleic Acids Res.* **37**, e45 (2009).
37. Stoddard, S. F., Smith, B. J., Hein, R., Roller, B. R. & Schmidt, T. M. rrnDB: improved tools for interpreting rRNA gene abundance in bacteria and archaea and a new foundation for future development. *Nucleic Acids Res.* **43**, D593–D598 (2015).
38. Muller, C., Birmes, F. S., Ruckert, C., Kalinowski, J. & Fetzner, S. *Rhodococcus erythropolis* BG43 genes mediating *Pseudomonas aeruginosa* quinolone signal degradation and virulence factor attenuation. *Appl. Environ. Microbiol.* **81**, 7720–7729 (2015).
39. Aleksashin, N. A. et al. A fully orthogonal system for protein synthesis in bacterial cells. *Nat. Commun.* **11**, 1858 (2020).
40. Khemaissa, S., Walrant, A. & Sagan, S. Tryptophan, more than just an interfacial amino acid in the membrane activity of cationic cell-penetrating and antimicrobial peptides. *Q Rev. Biophys.* **55**, e10 (2022).
41. Egan, A. J. F., Errington, J. & Vollmer, W. Regulation of peptidoglycan synthesis and remodelling. *Nat. Rev. Microbiol.* **18**, 446–460 (2020).
42. Heijenoort, van J. Recent advances in the formation of the bacterial peptidoglycan monomer unit. *Nat. Prod. Rep.* **18**, 503–519 (2001).
43. Egan, A. J., Biboy, J., van't Veer, I., Breukink, E. & Vollmer, W. Activities and regulation of peptidoglycan synthases. *Philos. Trans. R. Soc. Lond. B Biol. Sci.* **370**, 20150031 (2015).
44. Jordan, S., Hutchings, M. I. & Mascher, T. Cell envelope stress response in Gram-positive bacteria. *FEMS Microbiol. Rev.* **32**, 107–146 (2008).
45. Schmittgen, T. D. & Livak, K. J. Analyzing real-time PCR data by the comparative C_T method. *Nat. Protoc.* **3**, 1101–1108 (2008).
46. Joshi, N. A. & Fass, J. N. *Sickle: a sliding-window, adaptive, quality-based trimming tool for FastQ files (Version 1.33) [Software]*. https://github.com/najoshi/sickle, 2011).
47. Yu, G., Wang, L. G., Han, Y. & He, Q. Y. clusterProfiler: an R package for comparing biological themes among gene clusters. *Omics* **16**, 284–287 (2012).
48. Forli, S. et al. Computational protein-ligand docking and virtual drug screening with the AutoDock suite. *Nat. Protoc.* **11**, 905–919 (2016).
49. Pasquina-Lemonche, L. et al. The architecture of the gram-positive bacterial cell wall. *Nature* **582**, 294–297 (2020).

Acknowledgements

We thank J. Fan, M. Liu, X. Liu, and L. Chen from the Yingtan Agroecosystem Field Experiment Station of the Chinese Academy of Sciences for field experiment management and sampling assistance. We received funding from the National Natural Science Foundation of China (42425703 and 42377121 to Y.L., 42107146 to Z.M.), National Key R&D Program of China (2021YFD1900400 to Y.L.), the Natural Science Foundation of Jiangsu Province (BK20240015 to Y.L., BK20210994 to Z.M.) and the Youth Innovation Promotion Association of the Chinese Academy of Sciences (2016284 to Y.L.).

Author contributions

Y.L., Z.M., R.S., and J.Zhang conceptualized the study. Y.L., E.W., Y.B., J.Zhou, and R.S. developed the methodology. Y.L., Z.M., M.J., C.L., J.D., M.Y., S.S., Y.X., and H.Z. conducted the investigation. Z.M., M.J., C.L., J.D. M.Y., S.S., Y.X., H.Z., and Y.Y. curated the data. Y.L., Z.M., M.J., C.L., J.D., M.Y., and S.S. performed the formal analysis. Y.L., J.Zhou, R.S., and J.Zhang supervised the project. Y.L., Z.M., M.J., C.L., M.Y., and S.S. wrote the initial draft, and Z.M., M.J., C.L., J.D., M.Y., E.W., Y.B., S.S., J.Zhou, Y.X., H.Z., Y.Y., R.S., T.W.C., J.Zhang and Y.L. reviewed and edited the manuscript.

Competing interests

The authors declare no competing interests.

Additional information

Supplementary information The online version contains supplementary material available at https://doi.org/10.1038/s41467-024-54616-0.

Correspondence and requests for materials should be addressed to Yuting Liang.

Peer review information *Nature Communications* thanks Tengxiang Lian, Baogang Zhang and the other, anonymous, reviewer(s) for their contribution to the peer review of this work. A peer review file is available.